X-ray computed-tomography imaging of gas migration in water-saturated sediments: From capillary invasion to conduit opening

Jeong-Hoon Choi,[1] Yongkoo Seol,[1] Ray Boswell,[1] and Ruben Juanes[2]

Received 13 June 2011; revised 9 August 2011; accepted 10 August 2011; published 8 September 2011.

[1] The strong coupling between multiphase flow and sediment mechanics determines the spatial distribution and migration dynamics of gas percolating through liquid-filled soft granular media. Here, we investigate, by means of controlled experiments and computed tomography (CT) imaging, the preferential mode of gas migration in three-dimensional samples of water-saturated silica-sand and silica-silt sediments. Our experimental system allowed us to independently control radial and axial confining stresses and pore pressure while performing continuous x-ray CT scanning. The CT image analysis of the three-dimensional gas migration provides the first experimental confirmation that capillary invasion preferentially occurs in coarse-grained sediments whereas grain displacement and conduit openings are dominant in fine-grained sediments. Our findings allow us to rationalize prior field observations and pore-scale modeling results, and provide critical experimental evidence to explain the means by which conduits for the transit of methane gas may be established through the gas hydrate stability zone in oceanic sediments, and cause large episodic releases of carbon into the deep ocean. **Citation:** Choi, J.-H., Y. Seol, R. Boswell, and R. Juanes (2011), X-ray computed-tomography imaging of gas migration in water-saturated sediments: From capillary invasion to conduit opening, *Geophys. Res. Lett.*, *38*, L17310, doi:10.1029/2011GL048513.

1. Introduction

[2] Field observations suggest that gas transport through water-filled soft sediment is an essential component of seafloor dynamics, which controls natural gas seeps and vent sites [*Heeschen et al.*, 2003; *Best et al.*, 2006], the mechanical and acoustic properties of submarine sediments [*Anderson and Hampton*, 1980; *Waite et al.*, 2008], the creation of pockmarks in the ocean floor [*Hovland et al.*, 2002] and the viability of carbon dioxide sequestration in the sub-seafloor, either by hydrate formation [*Koide et al.*, 1995] or gravitational trapping [*Koide et al.*, 1997].

[3] Throughout the deepwater continental shelves, methane gas combines with pore waters to form gas hydrate. The morphology and distribution of hydrates provide clues as to the means of gas migration into the gas hydrate stability zone. Analyses of cores, many of which were obtained and imaged under *in situ* pressures, have revealed that gas hydrate occurrence is dominated by a pore-filling morphology in relatively coarse-grained sediments, whereas the mode of hydrate occurrence in typical marine clays is grain-displacing veins and fracture fills [*Holland et al.*, 2008; *Collett et al.*, 2009]. Recent analyses using pore-scale models are consistent with these observations, indicating that gas migration can occur as either capillary invasion or conduit opening, and that the crossover between the two processes depends chiefly on the pore size and the confining effective stress [*Jain and Juanes*, 2009; *Holtzman and Juanes*, 2010]. Fracturing or conduit opening, as a favored mechanism for gas release in fine-grained sediments, has been confirmed by 3D imaging in the lab [*Boudreau et al.*, 2005], and has recently helped explain the episodic methane venting commonly observed in freshwater lake sediments [*Scandella et al.*, 2011] and the ocean floor [*Heeschen et al.*, 2003].

[4] These gas invasion phenomena have important implications for understanding hydrates in natural systems (either ocean sediments or permafrost regions) [*Hornbach et al.*, 2004; *Weinberger and Brown*, 2006; *Uchida et al.*, 2009; *Daigle and Dugan*, 2010]. They suggest that, in fine sediments, hydrate will likely form as planar, grain-displacing veins, whereas, in coarse sediments, the buoyant methane gas will likely invade the pore space more uniformly and with minimal grain displacement, in a process akin to invasion percolation, causing hydrate in a pore-filling morphology. The nature of the accumulation response to environmental change (either natural or induced) may be dramatically different between the two regimes as well [*Boswell*, 2009].

[5] In this paper, we provide direct experimental evidence, by means of CT imaging of the mode of gas invasion in 3D sediment samples under controlled pore pressure and confining effective stress that are representative of ocean sediment conditions. Our experimental findings support the results of previously-reported pore-scale mechanistic models [*Jain and Juanes*, 2009; *Holtzman and Juanes*, 2010], which suggest the strong control of grain size on the nature of gas invasion into porous media.

2. Experimental Setup and Method

[6] We performed laboratory experiments of gas migration into water-saturated sediments with different median grain sizes (120 μm sand and 1.7 μm silt). We used synthetic silica sand (U.S. Silica, F110) and silica silt (U.S. Silica, Min-U-Sil-5), both with a composition of about 99% of silica quartz (Table 1). We use the term "silt" for the 1.7 μm sample, even though it falls in the grain-size range of a

[1]National Energy Technology Laboratory, Morgantown, West Virginia, USA.
[2]Civil and Environmental Engineering, Massachusetts Institute of Technology, Cambridge, Massachusetts, USA.

0094-8276/11/2011GL048513

Table 1. Physical Properties of Water-Saturated Samples, Pressure/Temperature Conditions During Gas Injection, and Ranges of Invasion Capillary Pressure at Initial Gas Migration

Parameter	Silica Sand	Silica Silt
Median grain size (μm)	120	1.7
Grain shape	Sub-angular	Angular
Sample size, diameter × length (mm)	39 × 109	39 × 112
Bulk density[a] (g/mL)	2.01	1.76
Porosity[a]	0.39	0.54
Outlet pore pressure, P_{out} (MPa)	6.90	7.58
Radial effective stress, σ'_r (MPa)	1.38	0.69
Axial effective stress, σ'_a (MPa)	2.62	1.31
Core temperature (°C)	20–22	20–22
Migration mode	Capillary invasion	Conduit opening
Invasion capillary pressure, P_c (MPa)	$0.04 < P_c \leq 0.07$	$0.41 \leq P_c \leq 0.62$

[a]Calculated from CT images.

"clay" (<2 μm), to avoid any misinterpretation that the sample has a clay mineralogy. Our experimental setup features x-ray CT scanners, and an x-ray transparent triaxial pressure vessel equipped with independent controls of pore pressure and confining stress in axial and radial directions. The experiments comprised four phases: (1) compaction of the sediment sample; (2) saturation of the pore-space with water; (3) injection of methane gas; and (4) post-gas injection CT scans.

[7] The two sediment samples, silica sand and silica silt, were compacted differently due to the different particle affinity to water. Oven-dried sand was mixed with water to achieve a water-to-sand mass ratio (g/g) of 0.13 before being packed into a rubber sleeve. Oven-dried silica silt was packed into the rubber sleeve without addition of water while the side wall of the rubber sleeve was clamped with three plastic blocks to constrain the sample dimension in the radial direction.

[8] The porosity of the sand sample under confining stresses is 0.39 (Table 1), which is within the typical range for natural sandy sediments (0.26–0.47) at depths typical of both arctic [*Winters et al.*, 2011] and marine [*Fujii et al.*, 2009] gas hydrate systems. The porosity of the silt sample is 0.54, which seems to be above the usual range of porosity values for natural silt-sized sediments, although very high nominal porosity values have been reported previously for natural sediments with substantial clay-size fractions [*Riedel et al.*, 2006]. The silt porosity may also be elevated due to insufficient compaction of silt particles or high angularity of the silt grains. Ensuring a dense granular pack for the rounder silica sand to avoid erosion and granular flow required compacting the sample down to a porosity of ~0.40, whereas it was not possible to pack the more angular silt grains to a porosity lower than 0.50 without creating cone-shape shear failure.

[9] The pressure vessel (Temco, Inc.) was connected to multiple syringe pumps to inject and withdraw fluid, and to apply axial and radial confining pressure. The sample inside the pressure vessel was incrementally pressurized by raising radial, axial and pore pressures up to the desired level (Table 1) while the ratio of radial-to-axial effective stress (= confining stress – water pore pressure) was held constant at 0.53 (Table 1). The samples were fully saturated with distilled water by sequential processes of CO_2 gas flushing (air

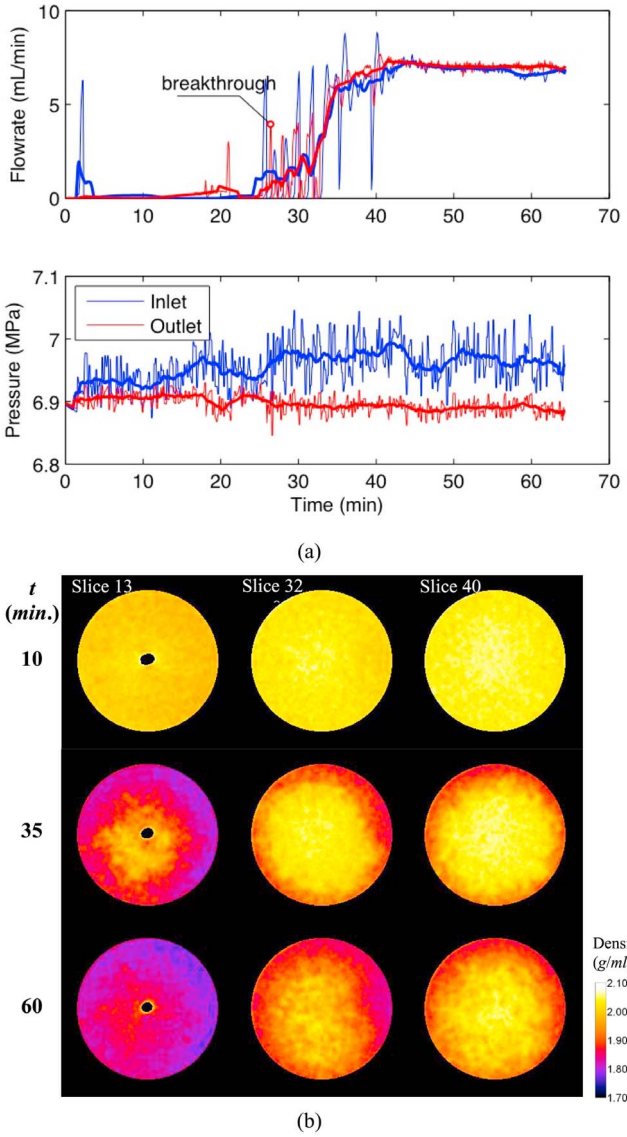

Figure 1. Invasion in silica sand. (a) (top) Time records of inflow (blue) and outflow (red) in the cell, and (bottom) inlet (blue) and outlet (red) pressures. The thicker lines denote a moving average over a window of 20 measurements. The outlet pressure is held approximately constant at around 6.9 MPa, while the gas injection pressure is progressively increased but then held approximately constant at a value less than 7.0 MPa. Shown in the flowrate time records is the time at which gas breaks through to the outlet. After this time, both inflow and outflow increase significantly, even though the pressure difference between inlet and outlet is approximately constant. (b) CT images at three different times (t = 10, 35, and 60 min) at three different locations within the cell – the slice number is counted in order from the sample end in fluid injection side. The black dot at the center of Slice 13 is from the gas injection tubing. Darker colors correspond to lower bulk densities, which indicate presence of gas in the pore space.

removal), pressurization (CO_2 liquefaction), water flushing, and pressure equilibration prior to gas injection.

[10] Methane gas was injected through a thin tubing (1.59 mm outer diameter) inserted 25 mm into the core sample within the horizontally-oriented pressure vessel. The gas injection pressure (P_{in}) was incrementally increased, while the back pressure at the outlet (P_{out}) was held constant at the equilibrated level. The main reason for point-source gas injection is to constrain the initiation of gas intrusion into the sample at a predictable location. When the gas is injected from a point source, it starts invading the sediment through pore throats where either the capillary entry pressure or grain contact compression is lowest [*Jain and Juanes*, 2009]. As gas injection continues, a more distributed pattern of gas develops in front of the point source, likely representing the natural setting in which gas migration occurs from distributed sources of gas supply.

[11] We conducted x-ray CT scanning between gas pressure increments to visually monitor the initiation, progress, and mode of gas migration. We used two x-ray CT scanners: a medical scanner (250 μm resolution, Universal Sys.) to observe initial or final conditions of the samples and gas migration patterns during gas injection, and a micro-CT scanner (4.1 μm resolution, Xradia, Inc.) to scan the samples after the injection test had been completed. Although the CT scanners do not permit imaging of individual pores, especially in the case of the silt sample, their resolution is sufficient to capture gas invasion patterns, which are often significantly wider than single pores. The full scan for the whole length of the specimen (about 55 slices, each of which was taken in 2-mm thickness) took just less than 6 minutes. Although the total scanning time is not much smaller than the characteristic flow time, the scan of individual slices (about 6 seconds) is.

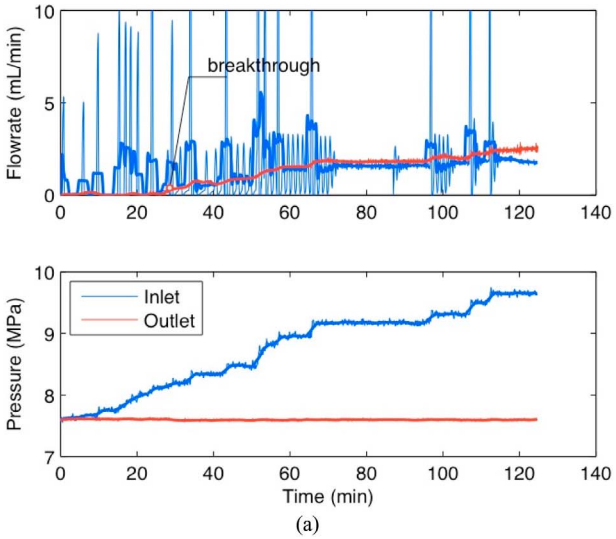

3. Results

3.1. Capillary Invasion of Gas in Silica Sand

[12] The gas injection (or inlet) pressure, P_{in}, was initially set to match the pore pressure of the water-saturated sand sample, which had been equilibrated to an outlet (or back) pressure, P_{out}, of approximately 6.9 MPa. The gas injection pressure is then progressively increased in small increments of about 20 kPa (Figure 1a). Although the experimentally-measured pressure record is noisy, we infer that the first gas invasion into the sample occurs at a capillary pressure (= gas pressure – water pressure) of about 40 kPa. In the absence of grain displacements and at low injection velocities, the invasion of a non-wetting phase (gas) into a porous medium saturated with a wetting phase (water) occurs when the capillary pressure exceeds the capillary entry pressure,

Figure 2. Invasion in silica silt. (a) (top) Time records of inflow (blue) and outflow (red) in the cell, and (bottom) inlet (blue) and outlet (red) pressures. The thicker lines denote a moving average over a window of 20 measurements. The outlet pressure is held approximately constant at around 7.6 MPa, while the gas injection pressure is progressively increased to values close to 10 MPa. The inflow time record exhibits sudden large spikes, which correlate with the times when the injection pressure is increased, irrespective of whether they occur before or after breakthrough of gas. (b) CT images at three different times (t = 23, 30, and 120 min) at three different locations within the cell – the slice number is counted in order from the sample end in fluid injection side. Darker colors correspond to lower bulk densities, which indicate presence of gas in the openings. Gas invasion involves large deformations of the sediment, which include the opening of conduits in a variety of morphologies (see text for a detailed description). (c) Micro-CT images of fine conduit openings in the silt sample. The images show the (left) top view and (middle and right) two cross-section views of a 3-D cylindrical volume rendered from the white-circled region shown in Slice 15 of Figure 2b at the end of gas invasion.

$P_c^e \sim 2\gamma/r_t$, where γ is the surface tension and r_t is the throat radius, which is of the order of one-tenth of the particle radius [*Hunt et al.*, 1988]. For a typical value of $\gamma \sim 0.07$ N/m and particle diameter $d_g \sim 120$ μm, we obtain $P_c^e \sim 25$ kPa, which agrees favorably with the value observed in the experiment.

[13] The CT images of selected slices of the sample at different times show that the invasion of gas throughout the sample takes place without any apparent formation of preferential conduits (Figure 1b). The gas invades first the region near the outer boundary, likely due to the slightly lower compaction around the edges of the sample or due to edge effects that result in larger pore openings near the outer boundary, as evidenced by the CT scans prior to gas invasion (Figure 1b, top). The CT images provide a clear picture of the macroscopic 3D distribution of gas throughout the sample. The cross-section averaged gas saturation decreases from inlet to outlet, consistent with a steady state in which the gas pressure decreases slightly along the length of the sample due to viscous resistance, and this decrease in capillary pressure results in a smaller fraction of the pores being accessible by exceeding the capillary entry pressure.

[14] Because of the low viscosity of the methane compared with that of water, there is a drastic increase in flowrate (mainly due to gas flow) once the gas breaks through to the outlet (Figure 1a, top). Taken together, all these observations demonstrate that gas migration in the sand sediment is controlled by capillary invasion.

3.2. Conduit Opening in Silica Silt

[15] We pre-equilibrated the water pore pressure at approximately 7.6 MPa, which was held constant at the outlet throughout the experiment. Gas was injected into the water-saturated silt sample by imposing increments in the inlet pressure (Figure 2a), just like in the sand sample. If gas were to invade by overcoming the capillary entry pressure corresponding to a nominal mean grain diameter $d_g \sim 1.7$ μm, the capillary pressure at the inlet would have to be raised to a value around $P_c \sim 1.6$ MPa. However, first gas invasion was detected near the injection tip at a value of the inlet capillary pressure of $P_c = P_{\text{in}} - P_{\text{out}} \sim 0.4$ MPa, significantly lower than the estimate from capillary invasion. Indeed, CT imaging confirms that gas invasion occurs by developing a conduit for preferential flow of gas (Figure 2b, top, slice 15).

[16] Analysis of the CT images taken at different cross sections of the sample throughout the course of the gas injection experiment suggests that conduit openings with different morphologies develop, which we classify into the following three types (Figure 2b): Type A, a planar or arcuate planar opening; Type B, an irregular spotty pattern; and Type C, longitudinally-oriented tube-shaped conduits shown as dark circles on the cross-sectional images. For example, the first detected invasion of gas (slice 15 at t = 23 min) corresponds to a Type-A feature. We interpret that Type-C openings (tube-type conduits) could originate from spots with a slightly lower packing density and from which silt particles could be more easily displaced laterally or longitudinally by methane gas flow. Type-C conduits also appear to dilate as gas continues to be injected through the sample with increasing inlet pressure (Figures 2a and 2b). Type B corresponds to features that seem to indicate flow focusing of gas, but from the 250-μm resolution medical scanner they could not be easily classified as fracture-like openings (Type A) or longitudinal conduits (Type C). CT scanning of selected areas of the silt sample with a higher-resolution (4 μm) micro-CT scanner revealed that the dark irregular spots seen in the medical-CT images (Type B) actually correspond to multiple fine fracture-like openings (Figure 2c).

4. Discussion and Conclusions

[17] Our controlled experiments of gas injection into two sediments of different grain size and *in situ* imaging by means of CT scanning confirm the transition in the mode of gas invasion, capillary invasion in coarse-grained media versus conduit opening in fine-grained media. The observed crossover from capillary invasion to conduit opening agrees with insights gained from pore-scale models [*Jain and Juanes*, 2009; *Holtzman and Juanes*, 2010], although those models (due to the many assumptions that are made) cannot predict with certainty the precise conditions (grain size and confining effective stress) under which the crossover will take place. Direct quantitative comparison of the results from the macroscopic experiments and the pore-scale models is challenging because the experimental system has: (1) a higher heterogeneity in grain size and, especially, throat size; and (2) a lower grain-contact compression and friction caused by the imperfections in the initial compaction and by the flexible lateral boundary (a rubber sleeve). For both of these items, the experimental setup likely mimics the natural conditions more closely than the numerical model.

[18] Our findings, obtained under controlled experimental conditions, are consistent with and allow us to rationalize prior field observations and modeling results indicating that gas hydrate (in areas of active gas migration) occurs in pore-filling mode in coarse-grained sediment, and primarily as networks of complex grain-displacing planar features in fine-grained sediment [*Holland et al.*, 2008]. Our observations also provide critical experimental evidence to explain the means by which gas may transit through the gas hydrate stability zone through new or reactivated pathways within fine grained-sediments [*Gorman et al.*, 2002; *Hornbach et al.*, 2004; *Weinberger and Brown*, 2006; *Daigle and Dugan*, 2010].

[19] **Acknowledgments.** We thank Karl Jarvis (URS) for technical support, Eilis Rosenbaum (NETL) for assistance with the micro-CT images and Carolyn Ruppel (USGS) for discussions. R.J. was supported by the U.S. Department of Energy under grant DE-FC26-06NT43067.

[20] The Editor would like to thank two anonymous reviewers for their assistance evaluating this paper.

References

Anderson, A. L., and L. D. Hampton (1980), Acoustics of gas-bearing sediments. 1. Background, *J. Acoust. Soc. Am.*, *67*(6), 1865–1889, doi:10.1121/1.384453.

Best, A. I., M. D. Richardson, B. P. Boudreau, A. G. Judd, I. Leifer, A. P. Lyons, C. S. Martens, D. L. Orange, and S. J. Wheeler (2006), Shallow seabed methane gas could pose coastal hazard, *Eos Trans. AGU*, *87*(22), doi:10.1029/2006EO220001.

Boswell, R. (2009), Is gas hydrate energy within reach?, *Science*, *325*, 957–958, doi:10.1126/science.1175074.

Boudreau, B. P., C. Algar, B. D. Johnson, I. Croudace, A. Reed, Y. Furukawa, K. M. Dorgan, P. A. Jumars, and A. S. Grader (2005), Bubble growth and rise in soft sediments, *Geology*, *33*(6), 517–520, doi:10.1130/G21259.1.

Collett, T. S., A. Johnson, C. Knapp, and R. Boswell (2009), Natural gas hydrates—A review, in Natural Gas Hydrates—Energy Resource Poten-

tial and Associated Geologic Hazards, edited by T. Collett et al., *AAPG Mem.*, 89, 146–220.

Daigle, H., and B. Dugan (2010), Origin and evolution of fracture-hosted methane hydrate deposits, *J. Geophys. Res.*, *115*, B11103, doi:10.1029/2010JB007492.

Fujii, T., T. Namikawa, T. Okui, M. Kawasaki, K. Ochiai, M. Nakamizu, M. Nishimura, O. Takano, and Y. Tsuji (2009), Methane hydrate occurrence and saturation confirmed from core samples, eastern Nankai Trough, in Natural Gas Hydrates—Energy Resource Potential and Associated Geologic Hazards, edited by T. Collett et al., *AAPG Mem.*, 89, 385–400.

Gorman, A. R., W. S. Holbrook, M. J. Hornbach, K. L. Hackwith, D. Lizarralde, and I. Pecher (2002), Migration of methane gas through the hydrate stability zone in a low-flux hydrate province, *Geology*, *30*(4), 327–330, doi:10.1130/0091-7613(2002)030<0327:MOMGTT>2.0.CO;2.

Heeschen, K. U., A. M. Trehu, R. W. Collier, E. Suess, and G. Rehder (2003), Distribution and height of methane bubble plumes on the Cascadia Margin characterized by acoustic imaging, *Geophys. Res. Lett.*, *30*(12), 1643, doi:10.1029/2003GL016974.

Holland, M., P. Schultheiss, J. Roberts, and M. Druce (2008), Observed gas hydrate morphologies in marine sediments, paper presented at the 6th International Conference on Gas Hydrates, Univ. of British Columbia, Vancouver, B. C., Canada.

Holtzman, R., and R. Juanes (2010), Crossover from fingering to fracturing in deformable disordered media, *Phys. Rev. E*, *82*, 046305, doi:10.1103/PhysRevE.82.046305.

Hornbach, M. J., D. M. Saffer, and W. S. Holbrook (2004), Critically pressured free-gas reservoirs below gas-hydrate provinces, *Nature*, *427*, 142–144, doi:10.1038/nature02172.

Hovland, M., J. V. Gardner, and A. G. Judd (2002), The significance of pockmarks to understanding fluid flow processes and geohazards, *Geofluids*, *2*, 127–136, doi:10.1046/j.1468-8123.2002.00028.x.

Hunt, J. R., N. Sitar, and K. S. Udell (1988), Nonaqueous phase liquid transport and cleanup: 1. Analysis of mechanisms, *Water Resour. Res.*, *24*(8), 1247–1258, doi:10.1029/WR024i008p01247.

Jain, A. K., and R. Juanes (2009), Preferential mode of gas invasion in sediments: Grain-scale mechanistic model of coupled multiphase fluid flow and sediment mechanics, *J. Geophys. Res.*, *114*, B08101, doi:10.1029/2008JB006002.

Koide, H., M. Takahashi, and H. Tsukamoto (1995), Self-trapping mechanisms of carbon dioxide in the aquifer disposal, *Energy Convers. Manage.*, *36*, 505–508, doi:10.1016/0196-8904(95)00054-H.

Koide, H., Y. Shindo, Y. Tazaki, M. Iijima, K. Ito, N. Kimura, and K. Omata (1997), Deep sub-seabed disposal of CO_2—The most protective storage, *Energy Convers. Manage.*, *38*, S253–S258, doi:10.1016/S0196-8904(96)00278-6.

Riedel, M., S. Collett, M. J. Malone, and the Expedition 311 Scientists (2006), *Cascadia Margin Gas Hydrates*, *Proc. Integr. Ocean Drill. Program*, vol. 311, Integr. Ocean Drill. Program, College Station, Tex.

Scandella, B. P., C. Varadharajan, H. F. Hemond, C. Ruppel, and R. Juanes (2011), A conduit dilation model of methane venting from lake sediments, *Geophys. Res. Lett.*, *38*, L06408, doi:10.1029/2011GL046768.

Uchida, T., A. Waseda, and T. Namikawa (2009), Methane accumulation and high concentration of gas hydrate in marine and terrestrial sandy sediments, in Natural Gas Hydrates—Energy Resource Potential and Associated Geologic Hazards, edited by T. Collett et al., *AAPG Mem.*, 89, 401–413.

Waite, W. F., T. J. Kneafsey, W. J. Winters, and D. H. Mason (2008), Physical property changes in hydrate-bearing sediment due to depressurization and subsequent repressurization, *J. Geophys. Res.*, *113*, B07102, doi:10.1029/2007JB005351.

Weinberger, J. L., and K. M. Brown (2006), Fracture networks and hydrate distribution at Hydrate Ridge, Oregon, *Earth Planet. Sci. Lett.*, *245*, 123–136, doi:10.1016/j.epsl.2006.03.012.

Winters, W., M. Walker, R. Hunter, T. Collett, R. Boswell, K. Rose, W. Waite, M. Torres, S. Patil, and A. Dandekar (2011), Physical properties of sediment from the Mount Elbert Gas Hydrate Stratigraphic Test Well, Alaska North Slope, *Mar. Pet. Geol.*, *28*(2), 361–380, doi:10.1016/j.marpetgeo.2010.01.008.

R. Boswell, J.-H. Choi, and Y. Seol, National Energy Technology Laboratory, 3610 Collins Ferry Rd., Morgantown, WV 26507, USA. (yongkoo.seol@netl.doe.gov)

R. Juanes, Civil and Environmental Engineering, Massachusetts Institute of Technology, 77 Massachusetts Ave., Bldg. 48-319, Cambridge, MA 02139, USA.